metals

MDPI

Article

The Effect of Severe Plastic Deformation on the Microstructure and Mechanical Properties of Composite from 5056 and 1580 Aluminum Alloys Produced with Wire Arc Additive Manufacturing

Aydar Mavlyutov [1,2,*], Alexey Evstifeev [1,3], Darya Volosevich [3], Marina Gushchina [1,3], Artem Voropaev [3], Oleg Zotov [4] and Olga Klimova-Korsmik [3]

[1] Mathematics and Mechanics Faculty, Saint Petersburg State University, Saint Petersburg 198504, Russia; ad.evstifeev@gmail.com (A.E.); skmar.spb@gmail.com (M.G.)
[2] Ioffe Institute, Russian Academy of Sciences, Polytekhnicheskaya Str. 26, Saint Petersburg 194021, Russia
[3] World-Class Research Center, State Marine Technical University, Saint Petersburg 190121, Russia; dasha.volosevich@mail.ru (D.V.); t-voropaev94@mail.ru (A.V.); o.klimova@ltc.ru (O.K.-K.)
[4] Institute of Metallurgy, Mechanical Engineering and Transport, Peter the Great Saint Petersburg Polytechnic University, Saint Petersburg 195251, Russia; zog-58@mail.ru
* Correspondence: a.m.mavlyutov@gmail.com

Abstract: In this study, a composite with alternate layers of 5056 and 1580 alloys was manufactured with wire arc additive manufacturing technology. It is shown that increased strength characteristics of composite material can be obtained with deformation treatment using a high-pressure torsion (HPT) technique. The microstructure and mechanical properties of the HPT-processed material in different structural states were investigated. The HPT-processed material exhibits a high value of ultimate tensile strength (~770 MPa) but low ductility. Short-term annealing at 250 °C and additional deformation with HPT to 0.25 of revolution at room temperature resulted in a slight decrease in the material's strength to ~700 MPa but provided ductility of ~9%. Physical mechanisms to improve plasticity in correlation with microstructure evolution are discussed.

Keywords: wire arc additive manufacturing; microstructure; mechanical characteristics; aluminum–magnesium alloys; aluminum–scandium alloys; ultrafine-grained structure

check for updates

Citation: Mavlyutov, A.; Evstifeev, A.; Volosevich, D.; Gushchina, M.; Voropaev, A.; Zotov, O.; Klimova-Korsmik, O. The Effect of Severe Plastic Deformation on the Microstructure and Mechanical Properties of Composite from 5056 and 1580 Aluminum Alloys Produced with Wire Arc Additive Manufacturing. *Metals* **2023**, *13*, 1281. https://doi.org/10.3390/met13071281

Academic Editor: Michael E. Kassner

Received: 19 May 2023
Revised: 25 June 2023
Accepted: 13 July 2023
Published: 17 July 2023

Copyright: © 2023 by the authors. Licensee MDPI, Basel, Switzerland. This article is an open access article distributed under the terms and conditions of the Creative Commons Attribution (CC BY) license (https://creativecommons.org/licenses/by/4.0/).

1. Introduction

Material processing using wire arc additive manufacturing (WAAM) technologies makes it possible to obtain various products from a wide range of metallic materials. The technology makes it possible to manufacture component parts with high precision, unique geometry, and material variety layer by layer. The undeniable advantage of this technology is the reduction of cost and production time in piece production [1]. The WAAM technology could be a unique tool for creating new materials with a given internal architecture that improves their mechanical and physical properties.

Aluminum–magnesium (Al–Mg) alloys are of particular interest within the scope of this study due to their numerous applications and desirable properties. These alloys are widely used in various industries, including aerospace, marine, and automotive, for their combination of low weight, high strength, and excellent corrosion resistance [2,3]. The excellent properties of Al–Mg alloys produced with additive manufacturing have been demonstrated by many scientific groups on a large number of different alloys, including 5056 [4,5], 5087 [6,7], 5183 [8], and 5356 [9,10].

WAAM technology offers numerous advantages in material processing; it also comes with certain shortcomings that must be considered during the assessment of its suitability

for specific applications. An extensive study of the effect of structural defects on mechanical properties was carried out by the authors in [11]. The main defect in the additive manufacturing of aluminum alloys is porosity, which inevitably degrades the mechanical properties of the material. As was shown, pores, reducing the loading area and the bearing capacity of the material, are places of crack nucleation during fracture [12]. In this regard, more attention should be paid to the study of porosity and its effect on the mechanical properties of additively fabricated aluminum alloys. In [11], the effect of WAAM + in situ interlayer rolling hybrid technology on the defect formation and mechanical properties of Al-4.5Mg–Mn alloy is studied. Interlayer rolling is found to be effective in reducing porosity—the number of defects after this treatment is four times lower than after conventional WAAM production. Moreover, interlayer rolling contributes to grain reduction from 59 μm to 23 μm. As a result, the material treated with interlayer rolling shows a 30% increase in relative elongation with practically unchanged strength properties.

Severe plastic deformation (SPD) methods could be one of the more extreme ways to improve the mechanical properties of WAAM materials. It is well known that SPD methods allow us to form a unique microstructure, providing extraordinary mechanical properties in bulk metallic materials [13]. Various SPD methods have been developed and examined in recent years; the results of these investigations have been analyzed and summarized in recent reviews [13–17]. It was shown that a nonporous structure with continuous layers, having high strength properties and acceptable plasticity, could be obtained from Ni/Ti [18] and Al/Cu [19] laminated composites with a cross-accumulative roll-bonding treatment. In recent years, many studies have been performed on SPD-processed pure aluminum and aluminum-based alloys [20–25]. It was shown that high-pressure torsion (HPT) processing results in the formation of an ultrafine-grained structure, providing high mechanical strength. Furthermore, in some cases, materials with enhanced mechanical strength demonstrate high ductility [24,25], although these are mutually exclusive properties for traditional metallic materials [26]. In [25], a new approach to improve plasticity while maintaining the high strength of HPT-processed commercially pure Al was proposed. This approach was based on the modification of the annealed structure of the high-angle grain boundaries by a slight additional deformation with HPT after short-term low-temperature annealing.

SPD methods have shown promising results in improving the mechanical properties of Al–Mg alloys. However, there are limitations to these methods that must be considered. The hardening of the Al–Mg alloys is due to the formation of a solid solution, as well as through deformation treatment. As was shown for equal-channel angular pressing (ECAP) processed Al–Mg alloys, an increase in Mg content from 0.5 to 2 wt.% leads to grain grinding and an increase in dislocation density [27]. The UFG Al–Mg alloys produced with HPT retained ductility at the acceptable level while Mg content is less than 2.5 wt.% [28]. A further increase in Mg content up to 4.1 wt.% results in the decrease of ductility of HPT-processed alloy [29]. Increased Mg content up to 4.5 wt.% completely suppresses plastic deformation in the HPT-processed material [28,29]. The thermal stability of nanostructured Al–Mg alloys remains unclear. One study found that Al–5Mg(wt.%) alloy treated with surface mechanical grinding has an enhanced thermal stability of mechanical properties up to 200 °C [30]. Another study found the degradation of mechanical properties of Al–5.5Mg(wt.%) alloy produced with ECAP with an increase in the annealing duration at 350 °C [31].

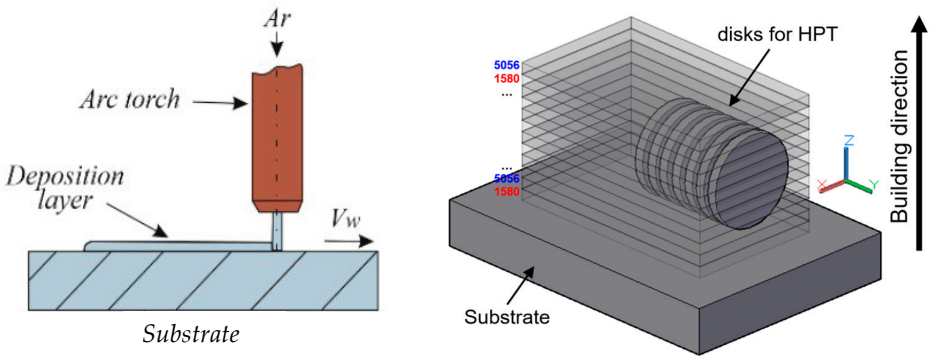
The problems mentioned above can be solved by the introduction of alloying additives into the UFG Al–Mg alloy that increases the strength and the recrystallization temperature. Among the alloying elements used in aluminum alloys, special attention is paid to Sc. It is one of the most effective modifiers, and even small Sc additives provide significant hardening and thermal stability [32–34].

In this work, an attempt to combine the WAAM and HPT processes for the creation of multilayer aluminum materials has been made. In this framework, the 5056 Al–Mg and 1580 Al–Mg(Sc) alloys were chosen as the materials for the investigation. The possibility of a

simultaneous increase in the strength and ductility of the HPT-processed composite with the additional deformation and heat treatment previously proposed in [25] was investigated.

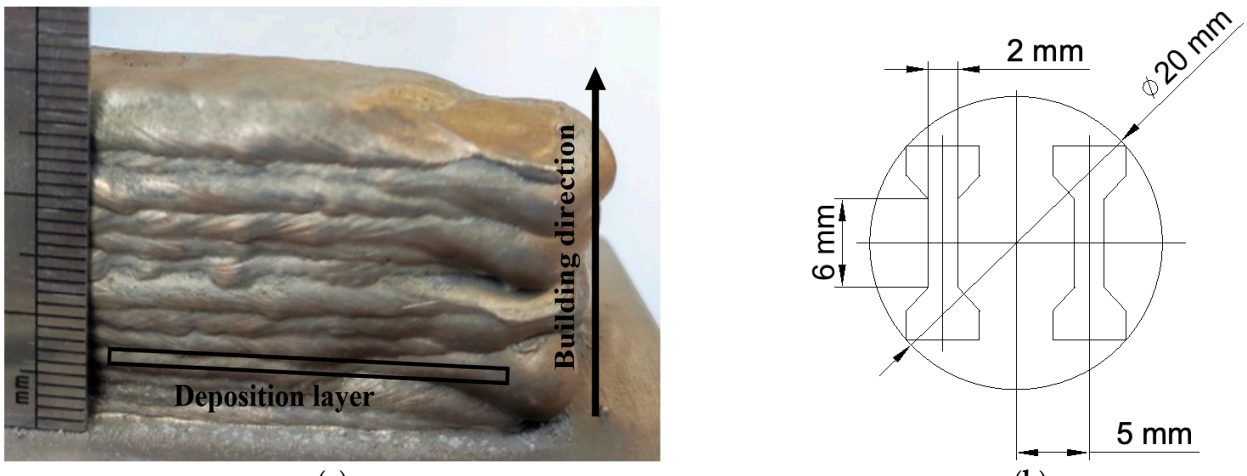
2. Materials and Methods

The materials for investigation were grown using a WAAM setup. The WAAM machine was based on the Fronius equipment package with cold material transfer technology. TPS 500i was used as a welding arc source. A Fanuc M-710ic industrial robot was used as a moving system. Samples were deposited using high-purity Ar shielding gas. Figure 1a shows a schematic representation of the deposition process. A series of preliminary tests were carried out to assess the sizes of individual weld beads as a function of the process parameters employed, including the deposition rate, current, and arc voltage. The bead geometry was considered when developing the robot's motion trajectory for each layer. The deposition was carried out at 120 A, 14.8 V, with a travel speed of 10–15 mm/s; the offset between adjacent beads was 3.2 mm. The wire feed was 8.1 m/min, and the diameter of the feedstock wire was 1.2 mm. The composite samples were obtained by depositing alternating layers of 5056 and 1580 aluminum alloys stacked on top of each other, with a thickness of each layer of 2.5 mm until the following final dimensions of the sample: 30 mm in height, 30 mm in width, and 100 mm in length. The schematic setup of the sample is shown in Figure 1b. The composite sample manufactured in this way is shown in Figure 2a. For HPT processing, disks with a diameter of 20 mm and a thickness of 1.5 mm were cut out from the sample according to the scheme (Figure 1b).



(**a**) (**b**)

Figure 1. Schematic representation of the deposition process (**a**); schematic setup of the sample obtained by depositing alternating layers of 1580 and 5056 aluminum alloys (**b**).



(**a**) (**b**)

Figure 2. Photo of the WAAM sample (**a**) and schematic representation of the dog-bone samples for mechanical tests (**b**).

The HPT processing of the disks was performed on the Walter-Klement HPT press to 10 revolutions at room temperature (RT) under a pressure of 6 GPa. After HPT processing, disks with a diameter of 20 mm and a thickness of ~1.0 mm were formed. The logarithmic strain of material at the middle of the disk radius was $e \approx 5.5$ [35]. Additional deformation heat treatment included annealing at 200–275 °C for 1 h and further HPT processing to 0.25 revolutions at RT under the same pressure, which corresponded to the extra logarithmic strain of $e \approx 1.5$ [35]. The annealing temperature was confirmed with a K-thermocouple placed next to the sample.

A chemical analysis of the 5056 Al–Mg and 1580 Al–Mg(Sc) alloys and the HPT-processed sample was performed using the scanning electron microscope (SEM) equipped with an Energy Dispersive X-ray (EDX) detector and the Oxford AZtec console (Oxford Instruments NanoAnalysis, Abingdon, Oxfordshire, United Kingdom).

XRD analysis was performed on a Bruker D8 DISCOVER diffractometer in symmetric θ–2θ scan modes using a parallel beam of CuKα radiation (40 kV, 40 mA). The scanning step was 0.02°, and the time of exposure was 0.5 s. The average size of the coherent scattering regions (C) and the level of microdistortions of the crystal lattice ($\langle \varepsilon^2 \rangle^{1/2}$) were determined via the full-profile Pauli simulation using the TOPAS 5.0 software. The dislocation density was calculated according to the following ratio [36]:

$$L_{dis} = \frac{2\sqrt{3}\langle \varepsilon^2 \rangle^{1/2}}{Cb}, \quad (1)$$

where b = 0.286 nm is the Burgers vector for edge dislocation in Al.

Transmission electron microscopy (TEM) was performed on an FEI Talos system equipped with a 200 kV field emission gun. Rapid TEM micrograph collection was undertaken at 25 frames per second while collecting 512 × 512-pixel images. Samples for TEM studies were prepared using a Mill TEM Model 1051 ion polishing machine.

Dog-bone samples with a gauge length of 6 mm and width of 2 mm were cut out from the disks according to the scheme (Figure 2b) using the electrical discharge machine. The average values of the yield stress ($\sigma_{0.2}$) corresponding to 0.2% of deformation, the ultimate tensile strength (σ_{UTS}), the relative elongation to failure (δ), and the relative uniform elongation (δ_1) were determined with the tensile tests at a constant strain rate of 5×10^{-4} s^{-1}. Fracture surfaces of the destroyed samples were studied using the SEM Zeiss AURIGA at the accelerating voltage of 10 kV.

3. Results and Discussion

The chemical composition, expressed in weight percentage (wt.%), of the 5056 Al–Mg and 1580 Al–Mg(Sc) layers in the sample obtained with WAAM and the composite produced with HPT is presented in Table 1. Upon examination, it becomes evident that the magnesium concentration in the HPT-processed composite is largely maintained at a level similar to that found in the initial 1580 alloy. However, a notable difference emerges in the concentration of scandium, which is considerably lower in the HPT-processed composite compared to the initial 1580 alloy. Additionally, the concentrations of other elements in the HPT-processed composite are observed to fall within the range between the concentrations found in the two initial alloys (5056 Al–Mg and 1580 Al–Mg(Sc)). This indicates that the HPT processing has led to a redistribution of the elements, resulting in a composite material that exhibits intermediate concentrations of these elements in comparison to the original alloys.

The stress–strain curves for the samples in different states of the composite can be seen in Figure 3. The initial state is characterized by a tensile strength on the level $\sigma_{UTS} \approx 265$ MPa and a high elongation to failure $\delta \approx 21\%$. This finding points to the high quality of the composite layered material, as the tensile tests were performed with the working part of the sample arranged perpendicular to the layers. This orientation ensures that the stress–strain curves reflect not only the strength of the individual layers but also the

adhesion between the materials, which differ in their chemical compositions. Furthermore, the high elongation to failure implies that the composite material has the potential for increased strength when subjected to SPD processing. After HPT processing, the ultimate strength of the material has tripled from ~265 to ~770 MPa, but at the same time, samples demonstrated brittle behavior. Such increased strength is attributed not only to grain refining (will be shown below) but also to the forming of magnesium segregations at grain boundaries, which affect the emission and mobility of intragranular dislocations and is typical for the Al–Mg alloys subjected to SPD [37,38].

Table 1. Chemical composition of 5056 Al–Mg, 1580 Al–Mg(Sc) alloys manufactured with WAAM method, and the HPT-processed composite, according to EDX analysis. The concentration is given in wt.%.

Material	Mg	Mn	Sc	Fe	Ti	Cr + V + Zn	Al
5056 alloy	4.94	0.14	-	0.09	0.14	<0.05	bal.
1580 alloy	4.61	0.55	0.08	0.17	0.1	<0.05	bal.
HPT-processed composite	4.66	0.27	0.03	0.11	0.12	<0.05	bal.

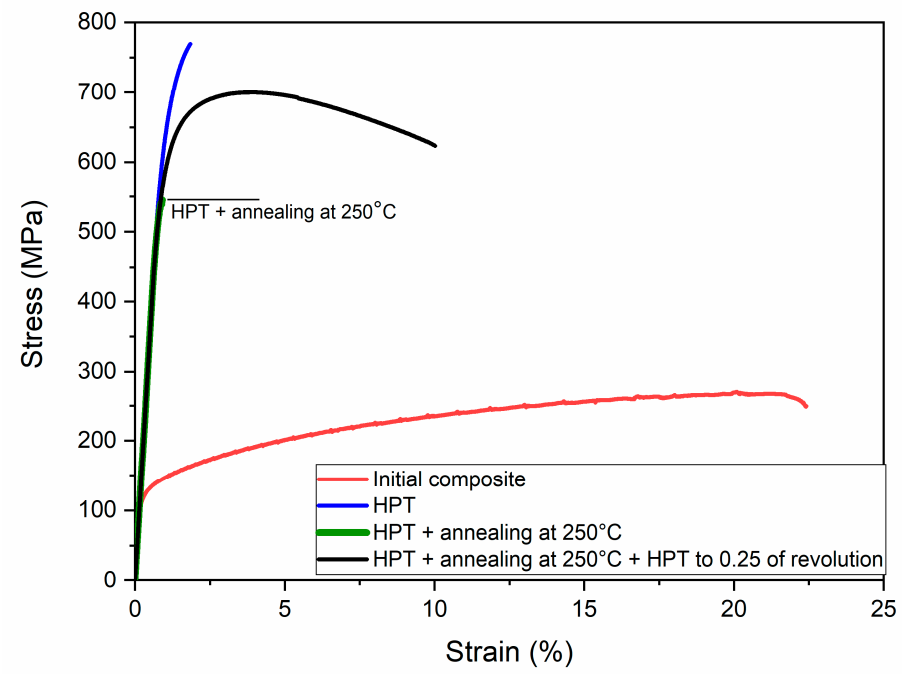


Figure 3. Stress–strain diagrams of composite in initial state, after HPT processing, after HPT processing and annealing at 250 °C for 1 h, after HPT processing, annealing at 250 °C for 1 h and additional HPT deformation to 0.25 revolutions.

Subsequent annealing of the HPT-processed material at 200–275 °C leads to even more embrittlement, and the sample was destroyed at the external stress ~504 MPa (Table 2). After additional deformation with HPT to 0.25 revolutions, the material demonstrates plasticity up to 10% (Figure 4). The best combination of tensile strength and plasticity was obtained after annealing at 250 °C and additional HPT to 0.25 revolutions. As a result, the yield stress ~590 MPa, ultimate tensile strength ~700 MPa, uniform elongation ~3%, and elongation to failure ~9% were obtained (Figure 4). The corresponding stress–strain curve is shown in (Figure 3). The results of the mechanical tests of the material in different structural states are summarized in Table 2.

Table 2. Mechanical properties of the composite in different structural states. $\sigma_{0.2}$ is the yield stress, corresponding to 0.2% of deformation, σ_{UTS} is the ultimate tensile strength, δ is the relative elongation to failure, δ_1 is the relative uniform elongation.

Composite Material State	$\sigma_{0.2}$, MPa	σ_{UTS}, MPa	δ, %	δ_1, %
Initial composite	132 ± 2	265 ± 5	21.0 ± 2.0	21.0 ± 2.0
HPT	676 ± 1	770 ± 2	~0.5	~0.5
HPT + annealing at 200 °C	–	611 ± 5	–	–
HPT + annealing at 250 °C	497 ± 2	504 ± 5	~0.2	~0.2
HPT + annealing at 200 °C + HPT to 0.25 of revolution	621 ± 2	667 ± 2	~1.0	~1.0
HPT + annealing at 225 °C + HPT to 0.25 of revolution	654 ± 2	733 ± 3	~2.0	~2.0
HPT + annealing at 250 °C + HPT to 0.25 of revolution	590 ± 1	700 ± 3	9.0 ± 1.0	~3.0
HPT + annealing at 275 °C + HPT to 0.25 of revolution	603 ± 2	666 ± 3	10.0 ± 1.0	~2.0

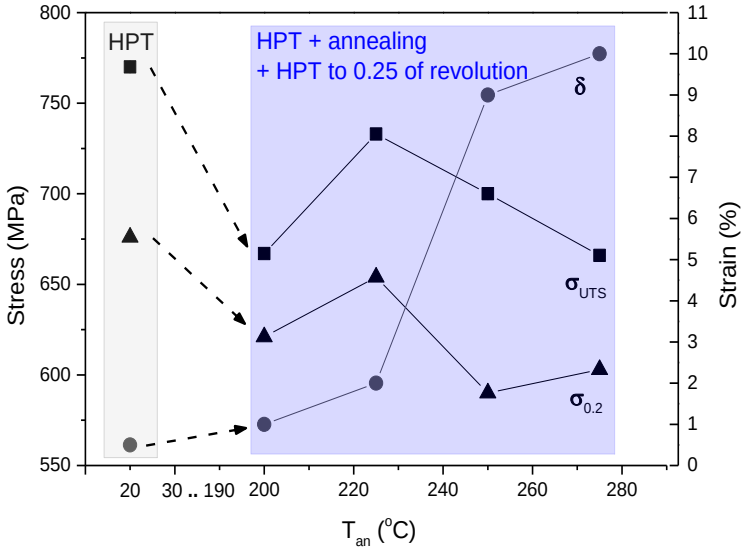


Figure 4. The dependences of ultimate tensile strength (σ_{UTS}), yield stress ($\sigma_{0.2}$), and elongation to failure (δ) on the annealing temperature for the composite samples, subjected to HPT, subsequent annealing and additional deformation with HPT to 0.25 of revolution.

The obtained mechanical properties are better than the properties of the 5083 alloy nanostructured with cryomilling, hot-isostatic pressing, and extrusion [39] and are higher than Al–5.55Mg alloy subjected to two passes of ECAP processing [31] and comparable with that for HPT-processed Al- 4.1Mg alloy [29].

The fracture surface of samples after HPT, annealing at 250 °C, and additional HPT processing is shown in Figure 5. The fracture surface of the HPT-processed material (Figure 5a,b) contains numerous micro- and macrocracks. Despite the severe destruction of the sample by a developed network of cracks, areas of plastic deformation still can be detected on the fracture surface (Figure 5b), which indicates that the material has some plastic capacity; nonetheless, uniform deformations do not exceed 1%. The fracture surface of sample after HPT processing and annealing at 250 °C is characterized by a brittle fracture with an extensive net of cracks along the surface of the working part of the sample (Figure 5c,d). There are no obvious traces of plastic deformation on the cracked

surface. These results fully correlate with X-ray analysis data showing the dislocation density reduction after annealing by an order of magnitude (Table 3). For Al-2.77% Mg alloy produced with ECAP, it was shown that the ductility of the alloy decreases with the increasing the number of ECAP processing passes [40]. The obtained final UFG structure demonstrates brittle destruction without the formation of necks. Subsequent annealing at 250 °C for 90 min does not lead to a change in the fracture behavior [40].

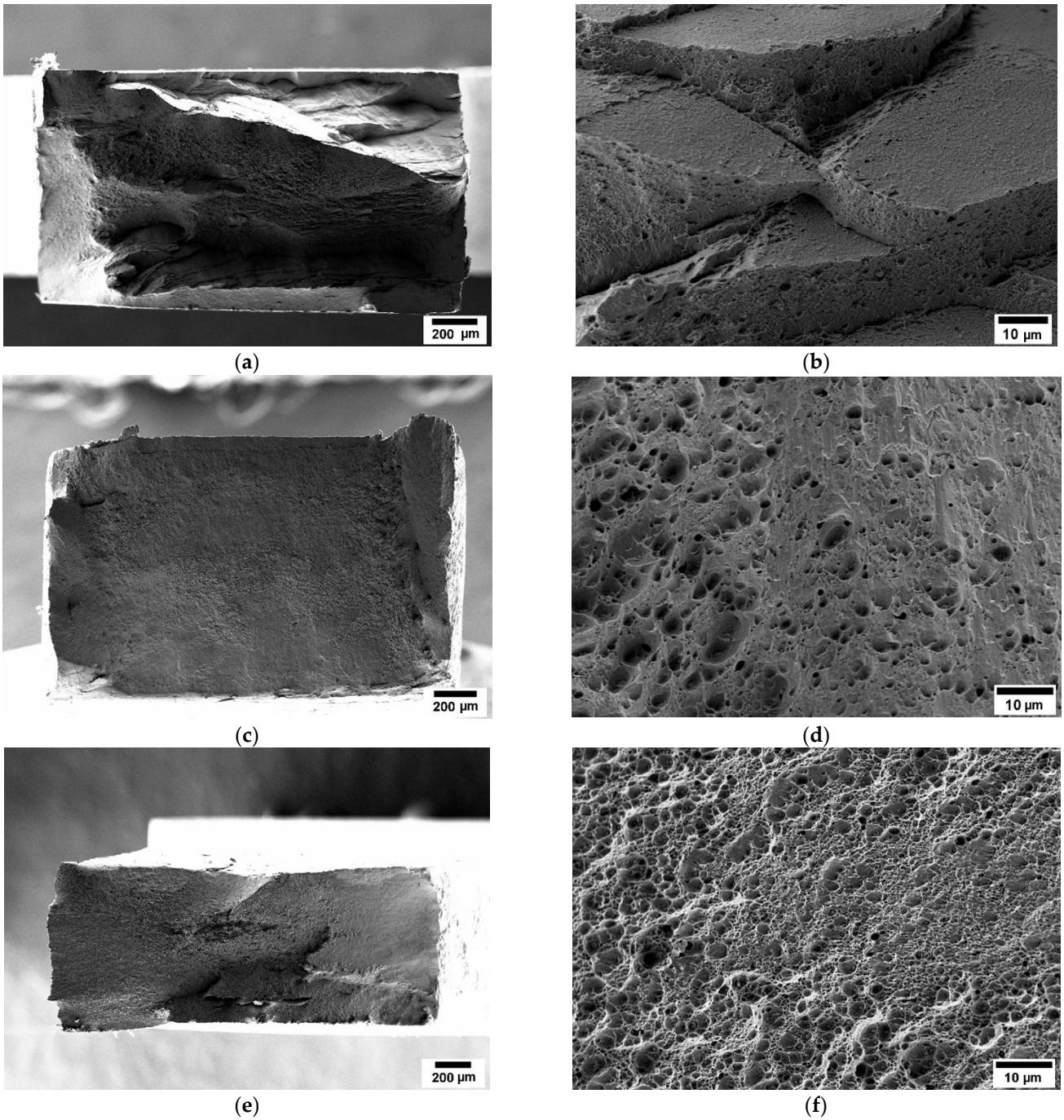


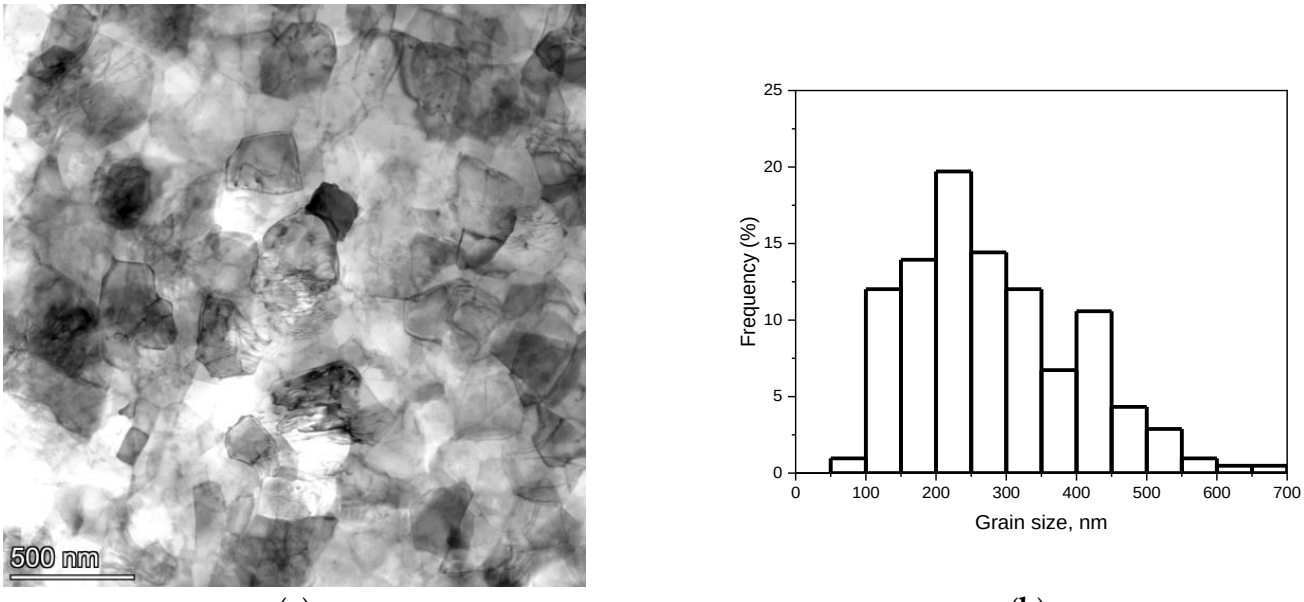
Figure 5. Fracture surface of the composite after HPT processing (**a**,**b**), after HPT processing and annealing at 250 °C for 1 h (**c**,**d**), after HPT processing, annealing at 250 °C for 1 h, and additional HPT deformation to 0.25 revolutions (**e**,**f**).

Table 3. Microstructure parameters of the composite in different structural states. *C* is the size of coherent-scattering domains, $\langle \varepsilon^2 \rangle^{1/2}$ is the elastic microdistortions level, L_{dis} is the dislocation density, d_{av} is the average grain size.

Composite Material State	*C*, nm	$\langle \varepsilon^2 \rangle^{1/2}$	$L_{dis} \cdot 10^{13}$ m^{-2}	d_{av}, nm
HPT	300	0.0013	5.2	285
HPT + annealing at 250 °C	470	0.0002	0.4	330
HPT + annealing at 250 °C + HPT to 0.25 of revolution	200	0.0010	6.0	160

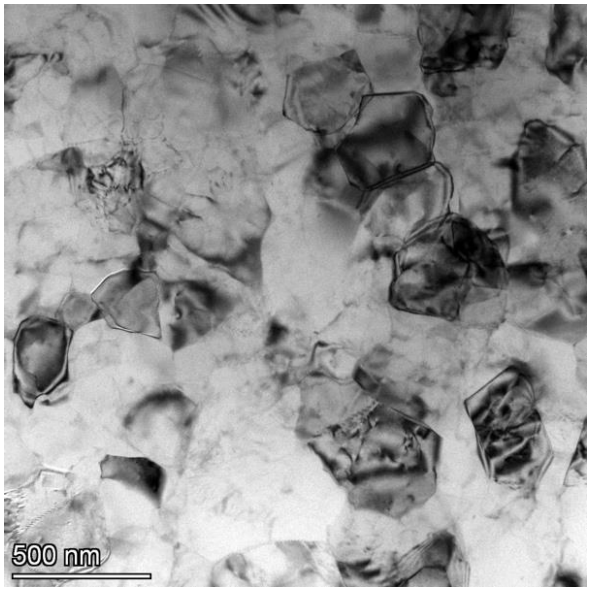
Additional HPT processing of the annealed structure leads to an increase in dislocation density and a decrease in coherent scattering regions (Table 3). On the fracture surface (Figure 5e,f), it is expressed by plastic deformation. The fracture surface is smoother and more homogeneous compared to the other structural states of the material.

The TEM microstructure images of the composite in different structural states are shown in Figure 6. As can be seen, an ultrafine-grained structure with uniaxial grains is formed upon HPT processing; there is no porosity in the structure (Figure 6a). The average grain size determined based on more than 100 measurements is $d_{av} \approx 285$ nm, which correlates with the size of coherent-scattering domains obtained with XRD analysis (Table 3). The selected area electron diffraction pattern (the insert in Figure 6a) reveals the high-angle misorientation of grains. The grain size has a normal distribution, which is shown in Figure 6b. As was shown earlier, the grain boundaries in the HPT-processed Al–Mg alloys are in a high-energy nonequilibrium configuration, containing a very high density of extrinsic dislocations, which gives rise to high internal stresses and high energies [41]. This may indicate that the dislocation density $L_{dis} \approx 5.2 \times 10^{13}$ m^{-2} estimated based on XRD analysis data refers to grain boundaries area.

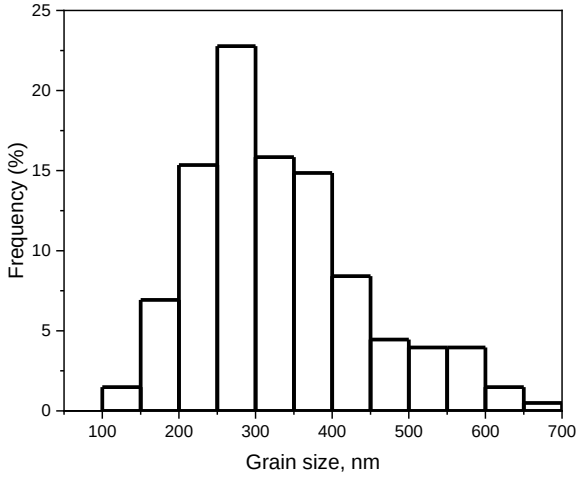


(**a**) (**b**)

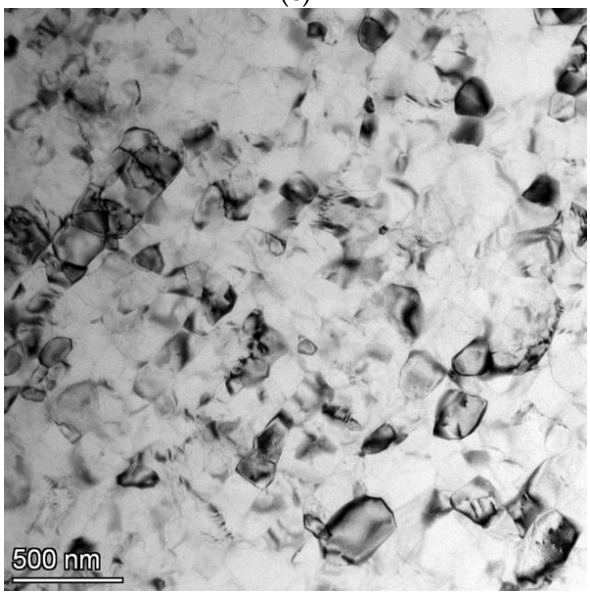
Figure 6. *Cont.*



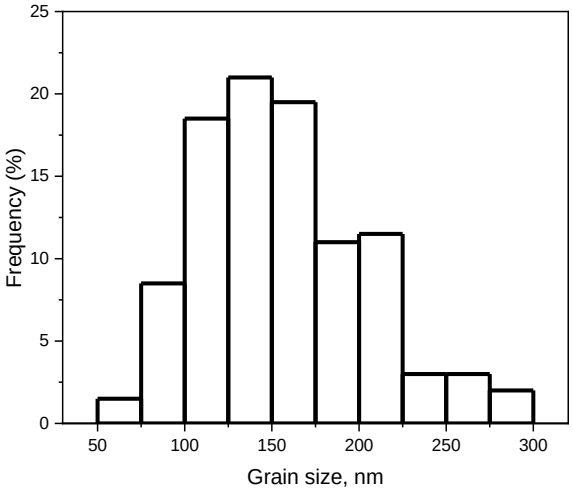
(**c**)



(**d**)



(**e**)



(**f**)

Figure 6. TEM micrographs of the composite after HPT processing (**a**), subsequent annealing at 250 °C (**c**) addition deformation with HPT to 0.25 of revolution (**e**), and corresponding grain size distribution (**b**,**d**,**f**).

After annealing at 250 °C, the average grain size and the distribution of grain size practically do not change (Figure 6c,d). This is in contrast with the results obtained with ECAP-processed Al-3.6Mg alloy, where annealing for 1 h at 250 °C led to the appearance of a duplex microstructure [42]. This means that the presence of Sc increases the thermal stability of the obtained structure. However, the results of the mechanical tests indicate reduced yield stress and ultimate tensile strength (Table 2) after annealing. Such a drop in strength after annealing is typical for conventional coarse-grained metallic materials but is usually accompanied by increased plasticity. The persistence of brittle behavior in our case may be associated with a restoration of grain boundaries expressed in a decrease in the number of mobile dislocations during annealing, as was revealed with XRD analysis (Table 3). Additional deformation with HPT to 0.25 of revolution results in grain refinement up to ~160 nm (Figure 6e, Table 3). The grain size distribution remains normal (Figure 6d).

According to the Hall–Petch ratio [43,44], grain boundary strengthening can be estimated as

$$\sigma_{GB} = k/\sqrt{d_{av}}, \quad (2)$$

where k = 0.1 MPa·m$^{1/2}$ is the material constant [16]. According to the ratio (2), grain refinement after additional deformation with HPT to 0.25 of revolution gives a contribution to grain boundary strengthening $\Delta\sigma_{GB} \approx 75$ MPa. Dislocation density increasing gives additional contribution to yield stress caused by the action of the dislocations strengthening mechanism [45]. The flow stress is related to the dislocation density with the Taylor equation [45]:

$$\sigma_{dis} = M\alpha Gb\sqrt{L_{dis}}, \quad (3)$$

where M = 3.06 is the Taylor factor [45], α = 0.33 is the dislocation interaction parameter [46], G = 26 GPa is the shear modulus.

Estimated on the basis of ratio (3), dislocations strengthening increase equal to $\Delta\sigma_{dis} \approx 40$ MPa. These two mechanisms, in total, provide practically the same strengthening as the experimentally observed increase in yield stress $\Delta\sigma_{0.2} \approx 93$ MPa. One of the main explanations of the manifestation of plastic properties after additional HPT processing can be given on the basis of the model proposed earlier in [47]: after additional deformation with HPT, the deformation-induced dislocations are formed in dislocation pile-ups in triple junctions of high-angle grain boundaries, increased plasticity occurs through the emission of lattice dislocations from triple junctions of grain boundaries, the glide of the lattice dislocations across neighboring grains, and their accumulation at and climb along the opposite grain boundaries. Apparently, the deformation–heat treatment that includes HPT, annealing at 250 °C, and additional torsion for 0.25 of revolution results in the formation of a unique structure with a small–average grain size and high density of dislocation pile-ups in the triple junctions of high-angle grain boundaries. Due to the performed annealing at 250 °C, the grain interior is free from forest dislocations, which allows unhindered emission of lattice dislocations and their glide across neighboring grains, thus realizing the mentioned mechanism of high plasticity. In previous work, the optimal annealing temperature was identified for HPT-processed commercial Al 5083 alloy [48]. As was shown, small additional deformation with torsion after annealing at 200 °C results in the formation of a structure with a unique combination of high strength and plasticity. In this paper, it is shown that the addition of Sc prevents the processes of grain boundaries' relaxation and dislocation redistribution. Therefore, the annealing temperature should be raised to obtain the required structural features.

4. Conclusions

The effect of SPD on the microstructure and mechanical properties of composite from 5056 and 1580 aluminum alloys produced with WAAM was studied. The following conclusions can be drawn:

(i) The ultimate strength of the HPT-processed material can reach ~770 MPa, which is ~3 times higher than the ultimate strength of the initial composite. Such a high level of strength is provided by the UFG structure with high dislocation density. However, the material exhibits low ductility, which is a limitation for many practical applications.

(ii) The combination of sufficient ductility and high tensile strength in the HPT-processed material was obtained by introducing an additional dislocation density with deformation–heat treatment consisting of short-term annealing at 250 °C and deformation with HPT to 0.25 of revolution at room temperature. The resulting material demonstrates a high tensile strength of ~700 MPa and an improved ductility of ~9%. Hereby, an effective way to improve the ductility of the material while maintaining a high level of strength was revealed.

(iii) The proposed combination of additive manufacturing and SPD suggests a high potential for practical applications of composite materials with high mechanical characteristics.

Author Contributions: A.M.: conceptualization, methodology, validation, analysis, supervision, writing—original draft, writing—review and editing. A.E.: investigation, data curation, visualization, XRD analysis and writing—original draft. D.V.: SEM and EDX analysis. M.G.: TEM analysis and editing. A.V.: participation in experimental work and visualization. O.Z.: participation in analysis and visualization. O.K.-K.: conceptualization, analysis and writing—review and editing. All authors have read and agreed to the published version of the manuscript.

Funding: This research was funded by Russian Science Foundation, grant number 22-79-10043. WAAM printing technology was implemented as part of the World-class Research Center program: Advanced Digital Technologies (Contract no. 075-15-2022-312 dated 20 April 2022).

Data Availability Statement: The data presented in this study are available on request from the corresponding author.

Acknowledgments: The mechanical and structural studies were performed using the equipment of the Laboratory for Mechanics of Advanced Bulk Nanomaterials for Innovative Engineering Applications of St. Petersburg State University and the "Interdisciplinary Resource Center for Nanotechnology" and the "Centre for X-ray Diffraction Studies" of the Research Park of St. Petersburg State University.

Conflicts of Interest: The authors declare no conflict of interest.

References

1. Ding, J.; Baumers, M.; Clark, E.A.; Wildman, R.D. The economics of additive manufacturing: Towards a general cost model including process failure. *Int. J. Prod. Econ.* **2021**, *237*, 108087. [CrossRef]
2. Mondolfo, L.F. *Aluminum Alloys: Structure and Properties*; Elsevier: Amsterdam, The Netherlands, 2013.
3. Aluminum Association. *Aluminum: Properties and Physical Metallurgy*; ASM International: Almere, The Netherlands, 1984.
4. Panchenko, O.; Kurushkin, D.; Mushnikov, I.; Khismatullin, A.; Popovich, A. A high-performance WAAM process for Al–Mg–Mn using controlled short-circuiting metal transfer at increased wire feed rate and increased travel speed. *Mater. Des.* **2020**, *195*, 109040. [CrossRef]
5. Salomatova, E.S.; Kartashev, M.F.; Trushnikov, D.N.; Permykov, G.L.; Olshanskaya, T.V.; Abashev, I.R.; Koleva, E.G. Evaporation processes of alloying components during wire-arc deposition of aluminum alloy 5056. *IOP Conf. Ser. Mater. Sci. Eng.* **2020**, *758*, 012064. [CrossRef]
6. Gu, J.; Ding, J.; Williams, S.; Gu, H.; Ma, P.; Zhai, Y. The effect of inter-layer cold working and post-deposition heat treatment on porosity in additively manufactured aluminum alloys. *J. Mater. Process. Technol.* **2016**, *230*, 26–34. [CrossRef]
7. Gu, J.; Wang, X.; Bai, J.; Ding, J.; Williams, S.; Zhai, Y.; Liu, K. Deformation microstructures and strengthening mechanisms for the wire-arc additively manufactured Al-Mg4.5Mn alloy with inter-layer rolling. *Mater. Sci. Eng. A* **2018**, *712*, 292–301. [CrossRef]
8. Zhang, B.; Wang, C.; Wang, Z.; Zhang, L.; Gao, Q. Microstructure and properties of Al alloy ER5183 deposited by variable polarity cold metal transfer. *J. Mater. Process. Technol.* **2019**, *267*, 167–176. [CrossRef]
9. Li, S.; Zhang, L.J.; Ning, J.; Wang, X.; Zhang, G.F.; Zhang, J.X.; Na, S.J.; Fatemeh, B. Comparative study on the microstructures and properties of wire-arc additively manufactured 5356 aluminum alloy with argon and nitrogen as the shielding gas. *Addit. Manuf.* **2020**, *34*, 101206. [CrossRef]
10. Wang, J.; Shen, Q.; Kong, X.; Chen, X. Arc Additively Manufactured 5356 Aluminum Alloy with Cable-Type Welding Wire: Microstructure and Mechanical Properties. *J. Mater. Eng. Perform.* **2021**, *30*, 7472–7478. [CrossRef]
11. Xie, C.; Wu, S.; Yu, Y.; Zhang, H.; Hu, Y.; Zhang, M.; Wang, G. Defect-correlated fatigue resistance of additively manufactured Al-Mg4.5Mn alloy with in situ micro-rolling. *J. Mater. Process Technol.* **2021**, *291*, 117039. [CrossRef]
12. Fu, R.; Tang, S.; Lu, J.; Cui, Y.; Li, Z.; Zhang, H.; Xu, T.; Chen, Z.; Liu, C. Hot-wire arc additive manufacturing of aluminum alloy with reduced porosity and high deposition rate. *Mater. Des.* **2021**, *199*, 109370. [CrossRef]
13. Zhu, Y.; Valiev, R.Z.; Langdon, T.G.; Tsuji, N.; Lu, K. Processing of nanostructured metals and alloys via plastic deformation. *MRS Bull.* **2010**, *35*, 977–981. [CrossRef]
14. Estrin, Y.; Vinogradov, A. Extreme grain refinement by severe plastic deformation: A wealth of challenging science. *Acta Mater.* **2013**, *61*, 782–817. [CrossRef]
15. Langdon, T.G. Twenty-five years of ultrafine-grained materials: Achieving exceptional properties through grain refinement. *Acta Mater.* **2013**, *61*, 7035–7059. [CrossRef]
16. Sabirov, I.; Murashkin, M.Y.; Valiev, R.Z. Nanostructured aluminium alloys produced by severe plastic deformation: New horizons in development. *MSEA* **2013**, *560*, 1–24. [CrossRef]
17. Kawasaki, M.; Langdon, T.G. Review: Achieving superplasticity in metals processed by high-pressure torsion. *J. Mater. Sci.* **2014**, *49*, 6487–6496. [CrossRef]
18. Liu, S.; Tayyebi, M.; Assari, A.H.; Polkowska, A.; Lech, S.; Polkowski, W. Microstructure, Texture and Tensile Properties of Nickel/Titanium Laminated Composites Produced by Cross Accumulative Roll Bonding Process. *Met. Mater. Int.* **2023**. [CrossRef]

19. Luo, J.; Khattinejad, R.; Assari, A.; Tayyebi, M.; Hamawandi, B. Microstructure, Mechanical and Thermal Properties of Al/Cu/SiC Laminated Composites, Fabricated by the ARB and CARB Processes. *Crystals* **2023**, *13*, 354. [CrossRef]
20. Talebanpour, B.; Ebrahimi, R.; Janghorban, K. Microstructural and mechanical properties of commercially pure aluminum subjected to dual equal channel lateral extrusion. *MSEA* **2009**, *527*, 141–145. [CrossRef]
21. Mavlyutov, A.M.; Bondarenko, A.S.; Murashkin, M.Y.; Boltynjuk, E.V.; Valiev, R.Z.; Orlova, T.S. Effect of annealing on microhardness and electrical resistivity of nanostructured SPD aluminium. *J. Alloys Compd.* **2017**, *698*, 539–546. [CrossRef]
22. Mavlyutov, A.M.; Kasatkin, I.A.; Murashkin, M.Y.; Valiev, R.Z.; Orlova, T.S. Influence of the microstructure on the physicomechanical properties of the aluminum alloy Al–Mg–Si nanostructured under severe plastic deformation. *Phys. Solid State* **2015**, *57*, 2051–2058. [CrossRef]
23. Huang, X.; Hansen, N.; Tsuji, N. Hardening by annealing and softening by deformation in nanostructured metals. *Science* **2006**, *312*, 249–251. [CrossRef] [PubMed]
24. Kamikawa, N.; Huang, X.; Tsuji, N.; Hansen, N. Strengthening mechanisms in nanostructured high-purity aluminium deformed to high strain and annealed. *Acta Mater.* **2009**, *57*, 4198–4208. [CrossRef]
25. Mavlyutov, A.M.; Latynina, T.A.; Murashkin, M.Y.; Valiev, R.Z.; Orlova, T.S. Effect of annealing on the microstructure and mechanical properties of ultrafine-grained commercially pure Al. *Phys. Solid State.* **2017**, *59*, 1970–1977. [CrossRef]
26. Valiev, R.Z.; Alexandrov, I.V.; Zhu, Y.T.; Lowe, T.C. Paradox of Strength and Ductility in Metals Processed by Severe Plastic Deformation. *J. Mater. Res.* **2002**, *17*, 5–8. [CrossRef]
27. Kalsar, R.; Yadav, D.; Sharma, A.; Brokmeier, H.G.; May, J.; Höppel, H.W.; Skrotzki, W.; Suwas, S. Effect of Mg content on microstructure, texture and strength of severely equal channel angular pressed aluminium-magnesium alloys. *MSEA* **2020**, *797*, 140088. [CrossRef]
28. Liu, M.P.; Roven, H.J.; Murashkin, M.Y.; Valiev, R.Z.; Kilmametov, A.; Zhang, Z.; Yu, Y. Structure and mechanical properties of nanostructured Al-Mg alloys processed by severe plastic deformation. *J. Mater. Sci.* **2013**, *48*, 4681–4688. [CrossRef]
29. Liu, Y.; Liu, M.; Chen, X.; Cao, Y.; Roven, H.J.; Murashkin, M.; Zhou, H. Effect of Mg on microstructure and mechanical properties of Al-Mg alloys produced by high pressure torsion. *Scr. Mater.* **2019**, *159*, 137–141. [CrossRef]
30. Xu, W.; Zhang, B.; Du, K.; Li, X.Y.; Lu, K. Thermally stable nanostructured Al-Mg alloy with relaxed grain boundaries. *Acta Mater.* **2022**, *226*, 117640. [CrossRef]
31. Snopiński, P.; Tański, T. Thermal stability and microstructure evolution of ultra-fine grained Al-Mg alloy. *IOP Conf. Series Mater. Sci. Eng.* **2018**, *461*, 012085. [CrossRef]
32. Konstantinov, I.L.; Baranov, V.N.; Sidelnikov, S.B.; Kulikov, B.P.; Bezrukikh, A.I.; Frolov, V.F.; Orelkina, T.A.; Voroshilov, D.S.; Yuryev, P.O.; Belokonova, I.N. Investigation of the structure and properties of cold-rolled strips from experimental alloy 1580 with a reduced scandium content. *Int. J. Adv. Manuf. Technol.* **2020**, *109*, 443–450. [CrossRef]
33. Konstantinov, I.L.; Baranov, V.N.; Sidelnikov, S.B.; Zenkin, E.Y.; Yuryev, P.O.; Belokonova, I.N. Influence of Rolling and Annealing Modes on Properties of Sheet Semifinished Products Made of Wrought Aluminum Alloy 1580. *Russ. J. Non-Ferr. Met.* **2020**, *61*, 641–645. [CrossRef]
34. Johansen, A. *Microstructures and Properties of Aluminium-Magnesium Alloys with Additions of Manganese, Zirconium and Scandium*; Norwegian University of Science and Technology: Trondheim, Norway, 2000; p. 230.
35. Zhilyaev, A.P.; Langdon, T.G. Using high-pressure torsion for metal processing: Fundamentals and applications. *Prog. Mater. Sci.* **2008**, *53*, 893–979. [CrossRef]
36. Williamson, G.K.; Smallman, R.E. III. Dislocation densities in some annealed and cold-worked metals from measurements on the X-ray debye-scherrer spectrum. *Philos. Mag.* **1956**, *1*, 34–46. [CrossRef]
37. Enikeev, N.A.; Murashkin, M.Y.; Sauvage, X.; Kazykhanov, V.U.; Valiev, R. SPD-induced grain boundary segregations and superior strength in UFG Al alloys. *Mater. Sci. Forum* **2011**, *667*, 665–669. [CrossRef]
38. Sauvage, X.; Enikeev, N.; Valiev, R.; Nasedkina, Y.; Murashkin, M. Atomic-scale analysis of the segregation and precipitation mechanisms in a severely deformed Al–Mg alloy. *Acta Mater.* **2014**, *72*, 125–136. [CrossRef]
39. Tellkamp, V.L.; Lavernia, E.J.; Melmed, A. Mechanical behavior and microstructure of a thermally stable bulk nanostructured Al alloy. *Met. Mater Trans A* **2001**, *32*, 2335–2343. [CrossRef]
40. Fang, D.R.; Duan, Q.Q.; Zhao, N.Q.; Li, J.J.; Wu, S.D.; Zhang, Z.F. Tensile properties and fracture mechanism of Al–Mg alloy subjected to equal channel angular pressing. *Mater. Sci. Eng. A* **2007**, *459*, 137–144. [CrossRef]
41. Horita, Z.; Smith, D.J.; Furukawa, M.; Nemoto, M.; Valiev, R.Z.; Langdon, T.G. An investigation of grain boundaries in submicrometer-grained Al-Mg solid solution alloys using high-resolution electron microscopy. *J. Mater. Res.* **1996**, *11*, 1880–1890. [CrossRef]
42. Morris, D.G.; Munoz-Morris, M.A. Microstructure of severely deformed Al–3Mg and its evolution during annealing. *Acta Mater.* **2002**, *50*, 4047–4060. [CrossRef]
43. Hall, E.O. The Deformation and Ageing of Mild Steel: III Discussion of Results. *Proc. Phys. Soc. B* **1951**, *64*, 747. [CrossRef]
44. Petch, N.J. The orientation relationships between cementite and α-iron. *Acta Cryst.* **1953**, *6*, 96. [CrossRef]
45. Hansen, N.; Huang, X. Microstructure and flow stress of polycrystals and single crystals. *Acta Mater.* **1998**, *46*, 1827–1836. [CrossRef]
46. Nabarro, F.R.N.; Basinski, Z.S.; Holt, D.B. The plasticity of pure single crystals. *Adv. Phys.* **1964**, *13*, 193–323. [CrossRef]

47. Orlova, T.S.; Skiba, N.V.; Mavlyutov, A.M.; Murashkin, M.Y.; Valiev, R.Z.; Gutkin, M.Y. Hardening by annealing and implementation of high ductility of ultra-fine grained aluminum: Experiment and theory. *Rev. Adv. Mater. Sci.* **2018**, *57*, 224–240. [CrossRef]
48. Evstifeev, A.D.; Smirnov, I.V. Effect of annealing and additional deformation on the microstructure and mechanical properties of ultrafine-grained Al5083 alloy. *Mater. Phys. Mech.* **2023**, *in press*.

Disclaimer/Publisher's Note: The statements, opinions and data contained in all publications are solely those of the individual author(s) and contributor(s) and not of MDPI and/or the editor(s). MDPI and/or the editor(s) disclaim responsibility for any injury to people or property resulting from any ideas, methods, instructions or products referred to in the content.